ELSEVIER

Coastal Engineering 41 (2000) 237–267

COASTAL ENGINEERING

www.elsevier.com/locate/coastaleng

Tide, wave and suspended sediment modelling on an open coast — Holderness

David Prandle [a,*], Julia C. Hargreaves [a], Julia P. McManus [a,1], Andrew R. Campbell [a], Kurt Duwe [b], Andrew Lane [a], Petra Mahnke [b], Susan Shimwell [c], Judith Wolf [a]

[a] *Proudman Oceanographic Laboratory, Bidston Observatory, Birkenhead, CH43 7RA, UK*
[b] *Hydromod Scientific Consulting, P.O. Box 1229, D-22880 Wedel / Holstein, Germany*
[c] *ARGOSS, P.O. Box 61, 8325 ZH Vollenhove, Netherlands*

Abstract

An intensive series of observations off the Holderness coast was followed by a related set of modelling applications. Observations included: aircraft and satellite remote sensing, H.F. and X-band radar, ship surveys and in situ instruments on the sea bed and at the sea surface. These observations aimed to monitor, over three successive winter periods, the dynamics and sediment distributions in the vicinity of this rapidly eroding coastline. Associated modelling applications included components simulating: (i) tides and surge currents; (ii) wave evolution; (iii) vertical distributions of turbulence and SPM (suspended particulate matter) and (iv) resulting spatial patterns of sediment transport in the region.

Simulations of tidal currents confirmed the accuracy of such models, given accurate fine-resolution bathymetry and appropriate boundary conditions. New developments of WAM, the spectral wave model required for fine-resolution applications in shallow water (described by Monbaliu et al. [Monbaliu, J., Padilla-Hérnandez, R., Hargreaves, J.C., Carretero Albiach, J.C., Luo, W., Sclavo, M., Günther, H., 2000. The spectral wave model WAM adapted for applications with high spatial resolution. This volume.]) are tested here. A number of additional features pertaining to shallow water are revealed including the sensitivity to specification of wind directions and the excessive temporal spreading of short-lived distant events. Likewise, the application of the generic

* Corresponding author. Fax: +44-151-653-6269.
E-mail address: d.prandle@pol.ac.uk (D. Prandle).
[1] Present address: Environment Agency (NE Region), Phoenix House, Global Avenue, Leeds, LS11 8PG, UK.

PII: S0378-3839(00)00034-X

single-point models for vertical profiles of turbulence and SPM (described by Baumert et al. [Baumert, H., Chapalain, G., Smaoui, H., McManus, J.P., Yagi, H., Regener, M., Sündermann, J., Szilagy, B., 2000. Modelling and numerical simulation of turbulence, waves and suspended sediment for pre-operational use in coastal seas. This volume]), are tested and also shown to be appropriate for simulating localised resuspension of SPM. This simulation also illustrates how, in shallow water (< 15 m), tidal and wave dynamics interact with significant mutual adjustments and with first-order influence on stress at the sea bed and thereby erosion and suspension processes.

Some preliminary simulations of net sediment movement are included, involving an integration of the above effects. These simulations emphasise how, in all but the shallowest water, the mobility of coarse grain sediments is limited to occasions of extreme waves. By contrast, the movement of fine sediments follows that of the residual tidal current streamlines, i.e., primarily longshore with attendant cross-shore dispersion. However, significant variation between closely-spaced observations indicates the irregularity and complexity of such distributions. It is concluded that because of the inability to prescribe the spatial distribution of available surficial sediments (including size distributions) such simulations can only be expected to reproduce the essential statistical characteristics of SPM concentrations. The availability of extensive remote sensing or in situ data can help to circumvent this problem.

Keywords: Coastal modelling; Coastal monitoring; Suspended sediment; Tides; Waves

1. Introduction

The broad objectives of this study were to quantify contemporary fluxes from a rapidly eroding coast to the adjacent sea and relate these fluxes to separate causative mechanisms via model simulations. The Holderness coast was chosen because of its rapid rate of erosion (20 m glacial till cliffs eroding at an average rate of 1.7 m year^{-1}) and its reasonable homogeneity over a 20-km section (Fig. 1). The observational requirement was for continuous monitoring of representative conditions over a winter period providing data both for developing and verifying numerical models of the region and background descriptions for occasional more intensive localised process studies.

The model simulations involved waves, tides, turbulence and SPM (suspended particulate matter) concentrations, including coupled models incorporating associated interactions. Results from component parts of the experiment have been reported elsewhere (the wave data set being adopted as a bench-test for model development internationally, Monbaliu et al., 2000). Here we report: (i) the essential characteristics of the tidal and wave dynamics including their interactions, (ii) incorporation of these components into a single-point models of turbulence intensity and SPM concentrations and (iii) a preliminary 2D (depth-averaged) model of SPM transport off Holderness.

Subsequent sections describe the observation experiments (Section 2); tidal modelling (Section 3); wave modelling (Section 4); modelling of vertical structure of SPM at a single point (Section 5) and spatial distributions of SPM off Holderness (Section 6). Summary and conclusions follow in Section 7. The extensive development in wave and SPM modelling is reflected in the greater emphasis given to Sections 4 and 5. By nature of the 3-year PROMISE project, these modelling components were under development simultaneously. A subsequent phase will address the rationalisation of common and

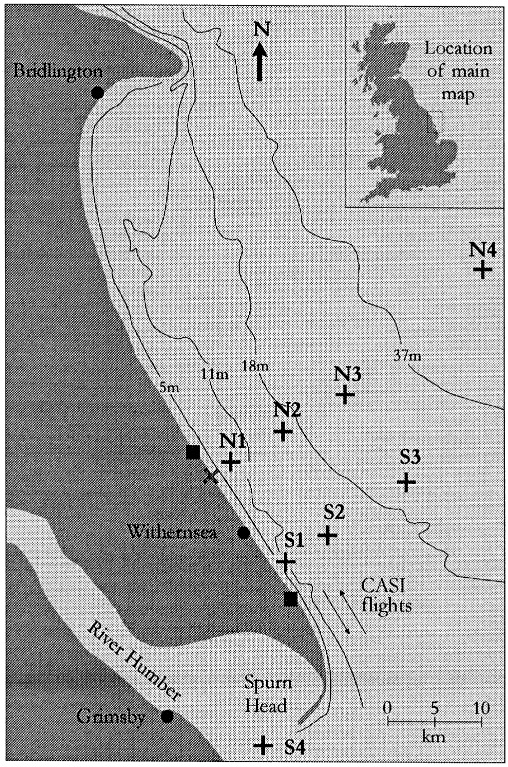

Fig. 1. Holderness Coast. Positions of moorings N1–N4, S1–S4.

interdependent aspects. Thus, while some disparities are evident, this paper serves to illustrate the complexity of integrating this range of component elements.

2. Observations

A comprehensive observational experiment aimed at quantifying sediment movement offshore of Holderness was undertaken for three successive winter periods. Currents, waves and concentrations of suspended particulate matter (SPM) were monitored by an array of in situ, radar and remote sensing instrumentation. This array of instrumentation used in the Holderness experiment is shown schematically in Fig. 2 (Prandle et al., 1996). Currents, wave parameters, pressure, temperature and conductivity were recorded by the instruments shown. Transmissometers and both optical and acoustic backscatter probes were used to measure SPM concentrations. Seven bottom-mounted POL (Proudman Oceanographic Laboratory) monitoring platforms (or PMPs) were deployed in two lines located perpendicular to the coast (Fig. 1) The PMPs were used to house: an ADCP (acoustic Doppler current profiler), an S4 electromagnetic current meter, a high-frequency water-level (pressure) recorder and a transmissometer. The rigs closest to the shore were

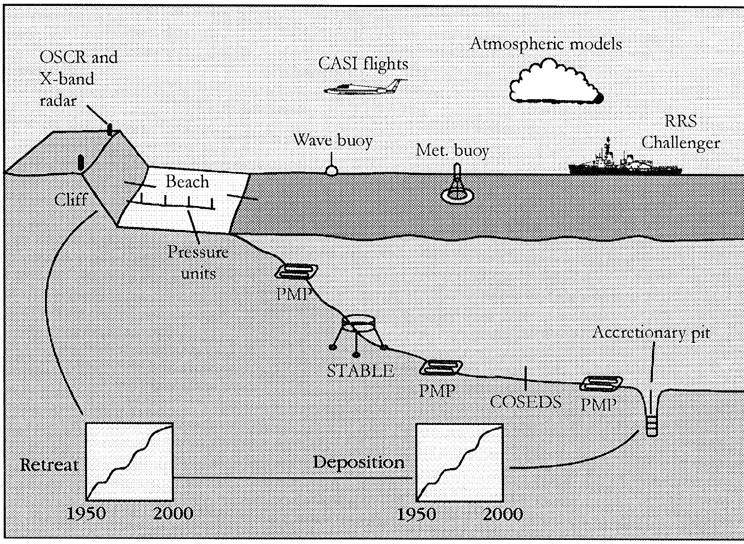

Fig. 2. Schematic of instrumentation deployed in the Holderness experiment.

equipped with the S4DW which included an OBS (optical backscatter). Acoustic backscatter (ABS) sensors were also used where available.

Other observations concurrent with these experiments included: the OSCR H.F. Radar system configured for measuring both surface currents and waves (Wyatt and Thompson, 1998); wave rider buoys at sites N1, N2 and N3 (Wolf, 1998); X-band radar, STABLE and regular CASI (compact airborne spectrographic imager) flights along the coast. Lane (1997) provides further details of the instrumentation deployed and summaries of the analysed data. Lane et al. (2000) provides detailed examples of recorded data.

3. Tidal modelling

Modelling of tidal propagation is well developed and hence only outline descriptions are included.

3.1. POL model

Depth-averaged tide and surge currents were simulated using a 1.2-km sub-grid model nested within the 12-km shelf-wide model CS3 developed at POL and used routinely by the UK Meteorological Office for surge forecasting. Reproduction of sediment movement away from the coast required the incorporation of a ‘wetting and drying’ module. The computed tidal ellipses showed close agreement with observed values, being predominantly semi-diurnal, essentially rectilinear aligned parallel to the coastline ($\approx 330°$). The predominant M_2 constituent amplitude is close to 45 cm s^{-1}, while the next largest S_2 has amplitude 12.5 cm s^{-1}, and N_2, 7–8 cm s^{-1}. The Z_0, or residual, constituent indicates a net southerly drift of typically 4.2 cm s^{-1}. Fig. 3

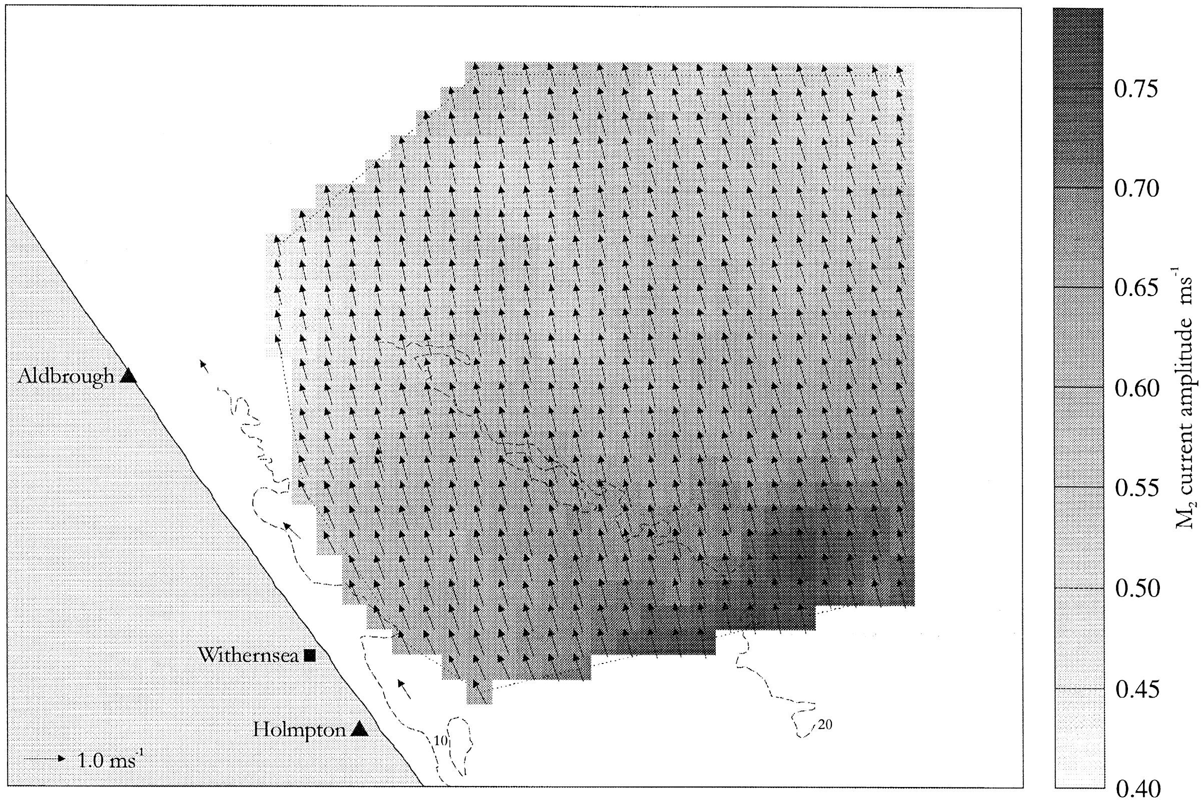

Fig. 3. Surface current ellipse amplitudes at Holderness for the M_2 constituent measured by OSCR H.F. radar from 17/12/95 to 15/1/96.

(Player, 1996) shows surface current ellipses for the M_2 constituent, obtained from H.F. Radar observations.

Surge currents are generally small in this area.

3.2. Hydromod models

In addition to the tidal and wave modelling described earlier and in Section 4, parallel studies were made by Hydromod as part of the PROMISE objective of model rationalisation. The Hydromod model is described by Duwe et al. (1983), the application to Holderness involved a 500-m grid with 10 vertical layers. Boundary conditions for this coastal model were provided from the North Sea/Baltic forecast model from the BSH, Hamburg. Wave data were obtained from the Deutsche Wetterdienst (DWD). The computed tidal currents agreed closely with observations and with values calculated by the POL model described in Section 3.1. An additional aspect of the Hydromod study was concerned with the sensitivity of tide-surge models to: (i) specification of winds and (ii) inclusion of waves.

Simulations concentrated on the periods October 1994 to January 1995. Sensitivity analyses were made of the effect on currents at N2 of (i) differing wind specifications and (ii) inclusion of wave interaction. The four simulations were as follows:

Case A.1: Wind field from DWD wave forecast model; no waves
Case A.2: Assimilated wind field for local Holderness model; no waves
Case B.1: Wind field from BSH North Sea model; no waves
Case B.2: Wind field from BSH North Sea model; wave information from DWD wave forecast model.

The DWD winds are on a coarser scale to that of the BSH. The wind field in Case A.2 is interpolated to the tidal model grid by Hydromod.

Table 1 indicates probability distributions for near-bottom currents at N2 corresponding to these four simulations. These results show little sensitivity to the precise specification of wind fields. Generally, surge currents are small in relation to tidal currents. By comparison, surface currents do indicate more pronounced sensitivity to wind fields. The influence of waves only slightly increases the occurrence of large

Table 1
Probabilities of near-bed currents at N2 for model simulations October 1994–January 1995

Current speed ($m\ s^{-1}$)	Case A.1 DWD wind (%)	Case A.2 Assim. Wind. (%)	Case B.1 BSH wind (%)	Case B.2 BSH wind + wave (%)
< 0.1	9.6	10.0	8.2	7.1
0.1–0.2	25.1	25.1	24.2	22.4
0.2–0.3	26.8	27.0	28.4	26.9
0.3–0.4	19.6	19.3	19.0	19.3
0.4–0.5	12.3	12.2	13.7	14.5
0.5–0.6	5.3	5.3	5.0	6.0
0.6–0.7	1.2	1.0	1.4	2.6
> 0.7	0.1	0.1	0.1	1.2

near-bed currents. This parallel model study emphasises that, away from the shallowest coastal regions, the impact of waves on tide-surge currents is second order.

4. Wave modelling

4.1. Model formulation

4.1.1. Background

For the purposes of modelling waves in all but very shallow water or other extreme conditions (e.g., large currents, rapidly shoaling bathymetry), it is generally assumed that all the processes that cause a change in the wave field interact only weakly with the wave field. This means that the wave field can be assumed to be a linear superposition of individual waves of different frequencies travelling in different directions. This gives rise to the frequency–direction spectrum and it is this spectrum which is modelled in WAM-Cycle4 (hereafter WAMC4, see Komen et al., 1994). It is not completely clear where the limit of applicability of models such as WAMC4 lies. For example, for depth refraction, linear theory requires $k \gg |\nabla h/h|$ where k is the wave number and h the water depth. In practical usage, however, the linear theory performs well down to $k \approx 3|\nabla h/h|$. Considerable effort has gone into developing WAMC4 for use in the shallow water areas studied in the PROMISE project. These developments are described in Monbaliu et al. (2000). With these developments in place, it has become reasonable to test the model for application up to the surf zone. Within the surf zone, waves are highly nonlinear and so linear theory cannot be expected to provide a reasonable model.

4.1.2. Bottom friction and sediment suspension

The motivation for modelling waves in PROMISE was the provision of accurate wave fields for input to sediment and turbulence models. It is the interaction of the waves and currents with the sea bed that causes sediment to be suspended. In addition, the interaction does also, of course, affect the waves themselves. In the wave model this appears as bottom friction dissipation. For accurate modelling, it is important that the bottom friction and sediment suspension terms are treated consistently between models and it is for this reason that some of the theory used in the models in regard to the bottom friction are outlined below.

According to van Rijn (1993), the bed shear stress due to a single wave is given by

$$\tau = \frac{\rho f_{\mathrm{w}} U^2}{4} \tag{1}$$

in which τ is the time-averaged bed shear stress, f_{w} is the friction coefficient and ρ is the fluid density. U is the magnitude of the orbital velocity at the top of the wave boundary layer and is given by

$$U = \frac{\pi H_{\mathrm{S}}}{T_{\mathrm{z}} \sinh(kh)} \tag{2}$$

where H_{S} is the wave height, and T_{Z} is the wave period.

There are various formulations for the friction coefficient depending on the nature of the flow. It is this formulation, in combination with the bed shear stress due to currents, that is used to derive the particle suspension in sediment models. The significant wave height and zero up-crossing period are used as approximations for H_S and T_Z. In the wave model, the dissipation due to bottom stress is calculated for each frequency of the wave energy spectrum. There are several parameterisations of the bottom stress in use in wave models. The default for WAMC4 is the Hasselmann (1968) drag law, and this is the configuration used for the modelling presented here, although through the PROMISE project several other parameterisations are now available (see Monbaliu et al., 2000). All the theories for the bottom stress result in formulae similar in form to the stress equation earlier in this section. The principal uncertainty is calculating the friction coefficient. The principal unknowns in ascertaining the value of friction coefficient are the bottom roughness and grain size. These parameters are, in general, not well known and are subject to change over the course of a model run as sea bed ripples form and are destroyed. It has been shown (Graber and Madsen, 1988) that the value of this coefficient can increase by an order of magnitude when the wave orbital velocity at the bed is sufficient to move the sea floor sediment. Dynamically coupled wave and sediment models may, in the future, prove to be a vital tool for understanding the interacting processes.

4.1.3. Holderness wave data

At POL, a version of WAMC4 developed through the PROMISE project (see Monbaliu et al., 2000) was implemented to study the waves over the Holderness region. A high quality wave data set was obtained during the experimental campaign at Holderness. The following details refer to the experiment covering the winter of 1994–1995. There were three Waveriders deployed in a line roughly perpendicular to the coast (Fig. 1). The Waverider buoy at N1 measured the frequency spectrum of the waves but gave no directional information. It was situated about 1 km offshore in an average water depth of 12.5 m of water; this varies by ± 3 m due to tide and surge over the period of the experiment. The buoys at N2 and N3 were both directional Waveriders meaning that directional information was obtained for each bin of the frequency spectrum. The buoy at N2 was about 5 km offshore in 18.3 m water depth and that at N3 was about 13 km offshore in 30 m of water. Spectra were obtained from N1 as an average over 2048 s every 1.5 h and at N2 and N3 as an average over 1600 s every 30 min.

The wave buoys were in sufficiently shallow water that only one compliant mooring could be used. This may lead to buoy resonance and hence wave energy overestimates at a frequency of 0.05 Hz. Very little wave energy was ever observed at this frequency so this is not a major source of error. The buoys are also known to miss the crest of the highest waves and hence underestimate them (Allender et al., 1989). The maximum significant wave height observed was 6 m and this should be well within the measuring range of the buoy. The buoys are generally assumed to have a random error of about 10% in the wave height.

There are several coastal wind stations on the East Coast of England. The one that provided the most continuous and frequent data was at Donna Nook, situated about 40 km south of N1. Average hourly wind speeds and directions were obtained from this station. While identical wind speeds would not be expected at Donna Nook and N1, the winds are useful as a guide to the accuracy of the model wind forcing.

Satellite altimetry from TOPEX/POSEIDON was also available and has been used for comparison with the results from the coarsest grid. These data had been corrected for the known bias in the significant wave heights (Krogstad and Barstow, 1999).

4.1.4. Model implementation

The scheme of nested grids is shown in Fig. 4. Model forcing was supplied by hourly wind data from the (UK Meteorological Office) UKMO Limited Area Model (spatial resolution approximately 50 km) interpolated onto the WAMC4 grids. The boundary conditions for the largest grid were full frequency–direction spectra taken at hourly intervals from the UKMO second-generation operational wave model. The row (or column) of the nearest UKMO points to each boundary was interpolated along the boundary from the model's 25-km resolution, 13 frequency and 16 directions bands to the 36-km resolution, 25 frequencies and 12 directions used in WAMC4.

Spectra were output from the large grid at the boundary of the first nested grid every 600 s (which was the time step of the large model). These boundary data were then interpolated in time and space by WAMC4 onto the boundary points of the nested grid, which had a resolution of 300 s in time and 12 km in space. In the same way, boundary

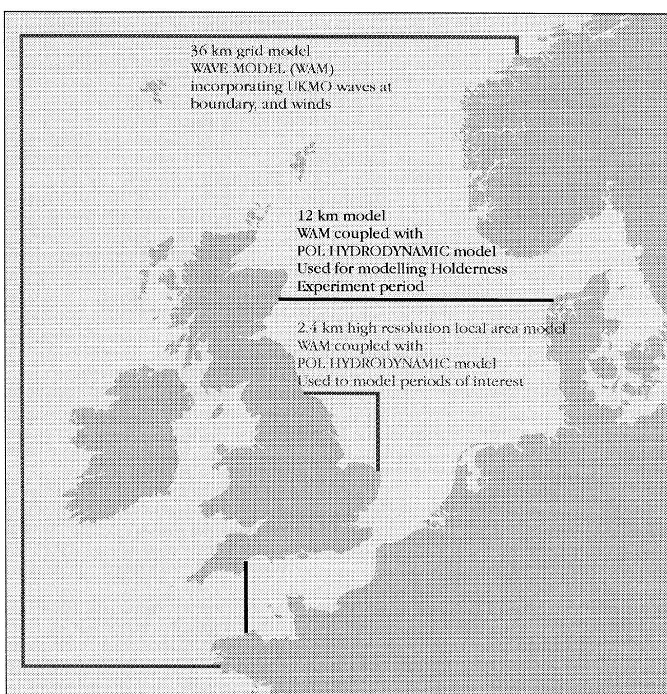

Fig. 4. The scheme of nested grids used to model the wave field at Holderness.

data for the finest, 2.4-km resolution, grid surrounding the Holderness region were produced from the first nested grid.

One of the developments of WAMC4 within PROMISE was the enabling of more flexibility in the choice of source and propagation time steps within the model. This allowed the fine grid to be run with a 60-s propagation time step and a 180-s source time step which permitted a 24-h model-time to be run in 3.5 h real-time on a workstation (HP712/100 MHz).

As well as the largest wave event observed at Holderness throughout the two winters of the experiment, the months of December 1994 and January 1995 contained a wide range of wave events with episodes of swell, wind sea and fetch limited growth. It is therefore these two months on which most of the wave modelling effort has been concentrated.

4.2. Results

The significant wave heights observed by the three buoys have been compared with the corresponding points in the model. N1 is a coastal boundary point in the model so is positioned at a fetch of 2.4 km, rather than 1 km. In the model the water depth was 11 m at N1, 14 m at N2 and 28 m at N3.

4.2.1. Significant wave height

A commonly used measure of error in the significant wave height is the Scatter Index (SI). This is defined as the root mean square difference between modelled and measured results divided by the mean of the measurements. The result obtained from the SI is, however, dependent upon the wave conditions being modelled. Furthermore, the value of the SI is more heavily weighted by the errors on the higher wave heights. In an attempt to remove this bias from the statistics, we consider the variation of the difference between model and buoy output with significant wave height. Fig. 5 shows the difference between model and buoy results at N1, N2 and N3 plotted as a function of the significant wave height as measured by the buoys. The data for each buoy were split into four quartiles according to significant wave height (H_S), and the mean and standard deviation of the difference between model and buoy wave heights were calculated for each quartile. Both the mean differences and standard deviations of the differences increase with increasing wave height, but not simply as a percentage of the wave height. The model consistently underestimates the wave height at all three stations although this error is less at N1 than at the other three sites. The best-fit straight line for N2 and N3 together is

$$\overline{H_{SB} - H_{SM}} = 0.13 \times \overline{H_{SB}} - 0.043 \tag{3}$$

and the best fit line for N1 is

$$\overline{H_{SB} - H_{SM}} = 0.23 \times \overline{H_{SB}} - 0.057 \tag{4}$$

where $\overline{H_{SB}}$ and $\overline{H_{SM}}$ are the buoy and model significant wave heights. The values derived by this method gave the same values as linear least squares fitting to the whole

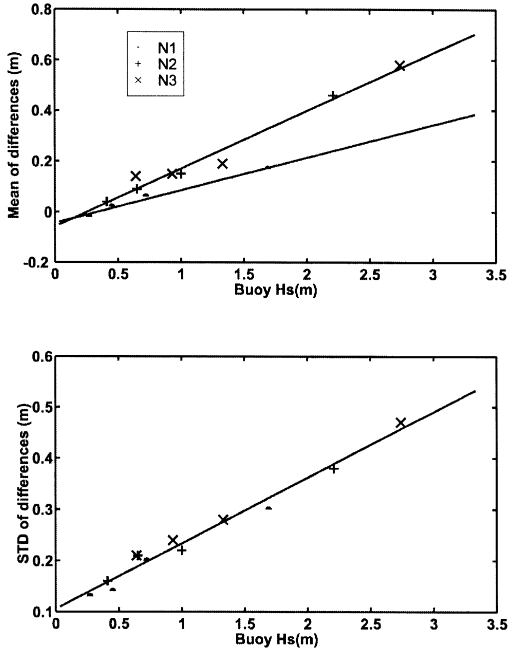

Fig. 5. Comparison of buoy and model significant wave heights at N1, N2, and N3 for a 2-month run. The 'differences' are the buoy wave heights minus the model wave heights.

data set. It is, however, only by splitting up the results in some way that the variation of the standard deviation can be estimated. The best fit straight line is given by

$$\mathrm{STD}\left(\overline{H_{\mathrm{SB}} - H_{\mathrm{SM}}}\right) = 0.13 \times \overline{H_{\mathrm{SB}}} + 0.11 \tag{5}$$

The error on the wave buoy measurements is expected to be a random variation of about 10% of the wave height rather than a bias, so we can consider the bias to be almost all due to model error. Since random errors add in quadrature, it is also true that the standard deviation given above is mostly due to model error. It should be pointed out that when modelling accuracy becomes more comparable with the buoy accuracy, a more sophisticated error analysis, which takes into account the buoy error statistics, would be required.

These results give us a guide to the overall performance of the model in the Holderness region. For example, a typical wave field of about 1 m significant wave height at N3, the modelled wave height is expected to be 0.9 ± 0.2 m to one standard deviation. However, for a very large 7-m event the modelled wave height would be 6.1 ± 1 m.

4.2.2. Event analysis

The global statistics derived above indicate how well the model is performing on average but do not help much in pinning down the sources of error. There are several ways in which inaccuracy can occur in WAMC4. There may be errors in the boundary spectra or winds forcing, or the imperfect representation of the growth, dissipation or propagation of the waves may cause errors. More information may be gleaned from the model results, however, through inspection of the whole wave spectra for particular characteristic wave events. Some examples of this approach are given in the next section.

4.2.2.1. A big storm. The storm of the 1st–3rd January 1995 produced the largest significant wave height seen at the buoy stations throughout the periods of the experiment. Events such as these should produce large amounts of suspended sediment in the shallow waters and so are the most important for accurate modelling of sediment transport.

Fig. 6 shows a snapshot during the storm (at 18:00 on 1st January 1999) as modelled by WAMC4 and observed by the wave buoys. The plot of energy spectra shows that the model significantly underestimated swell at N3, but the model result was improved at N1. Both these features are typical for swell events observed over the two months of the model run. The model improvement at N1 has a simple explanation. Since N1 was only in 12.5 m of water, dissipation of the wave energy due to bottom friction was a

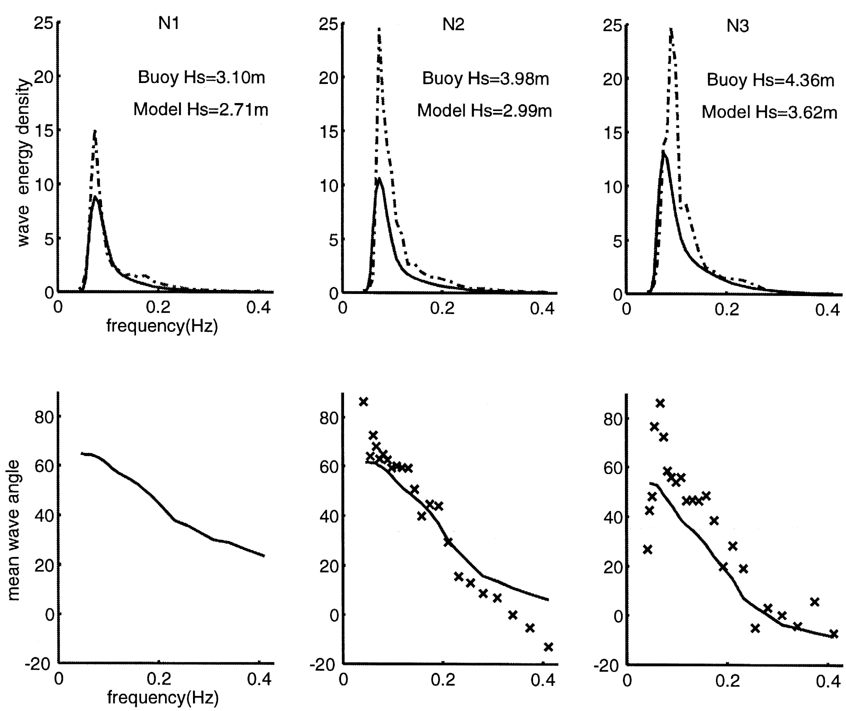

Fig. 6. Wave spectra during the big storm, at 18:00 on 01/01/1995. The model results are the solid lines and the buoy results are the dot-dashed lines in the top plots and the crosses in the bottom plots. An angle of 90° is directly onshore whereas 0° is along shore from south.

dominant process. The amount of bottom friction is dependent on the amount of wave energy, so bigger waves will be dissipated more than smaller ones and the buoy and model results would be expected to converge in shallower water.

On the plots of mean angle against frequency, 90° is approximately onshore and 0° indicates waves coming from west of north approximately parallel to the coastline. There was evidence of wave refraction in both the model and buoy results. This can be seen by comparing the mean angle of propagation for the spectral peak at N3, N2 and N1. It is also interesting to note that the longer frequency waves are clearly refracted more than the shorter waves in deep water. The diagram also shows that there was much more scatter in the buoy directions than in the buoy frequency spectrum, particularly at low wave energy.

The underestimate of swell was a persistent problem over the model run. There are several possible causes for the error. It is possible that the waves at the boundary of the coarse grid may have been underestimated. To check this effect, the coarse grid model results were compared with the satellite altimeter wave heights. Information from the satellite is temporally and spatially sparse so an average was calculated for the whole two months of the model run. The model, on average, underestimates the significant wave heights over the whole grid by about 15%. This value does not change significantly between the north edge of the grid and the middle of the North Sea. Supposing one had a perfect model with perfect wind forcing, then an underestimate of the boundary conditions should produce errors in the result which decreases from the boundary. Since this was not the case for this run, the indication is that other factors are also important. Other possible contributing factors are inaccuracy and smoothness in the winds driving the model and smoothing errors caused by the diffusive propagation scheme. The model winds are smooth on the scale of about 6 h and about 200 km. Hargreaves and Annan (1999) demonstrated how this, in combination with the smoothing of the propagation scheme, can lead to the underestimate of peak events in model results.

Another interesting characteristic of the wave field during this particular storm is the periodic variation of the significant wave height measured by the buoy, which is not reproduced by the model. This feature is particularly obvious at N1 and N2 as shown by Fig. 7. A Morelet wavelet transform of the buoy wave heights was performed for the whole two months of the run. The 12.5-h period, which is indicative of the changing depths and currents associated with the tides, was frequently evident throughout the run at N1. The only time over which the signature was identified at N3 was around this storm event, from 1st –6th January 1995. This was also the only period when waves greater than 3 m were sustained for several days at N3.

4.2.2.2. Wind-sea from the south. There are several occasions during the model run when a large part of the wave energy in the spectrum appears, in the buoy measurements, to be coming from the South. This bump of energy is frequently missing from the wave model results. Fig. 8 shows an example of this. The peak frequency of the wave energy corresponds to a fairly local event. In these cases, the winds as measured at Donna Nook are more southerly than those driving the model at N1. As illustrated in Fig. 1, the coastline onshore from the wave buoys is at an angle of about 45°. The

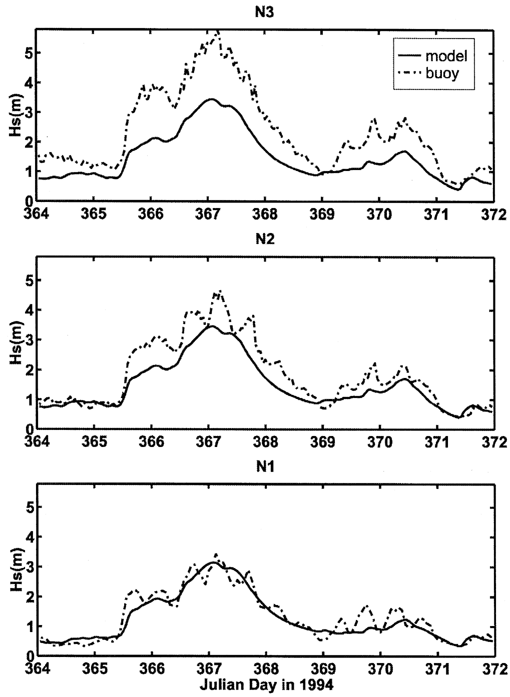

Fig. 7. Significant wave heights for the period covering the whole storm event. Regular oscillations in the buoy data are obvious by eye at N1 and N2.

southern most tip of this straight part of the coastline (Spurn Head) is close to due south of N3. This means that waves coming from the south experience a significantly greater fetch to those growing offshore from the Holderness coast, and so larger waves would be expected for the same wind speed. This is in agreement with our observation except that the wind at Donna Nook in these cases is often too westerly for waves travelling in a straight line to reach N3. It would be expected, however, for waves forced by wind from slightly west of south to be refracted round past Spurn Head and travel towards N3. These waves should appear in the spectrum to be travelling from a more southerly direction (closer to along shore) than the wind direction, as observed.

Three examples of this effect are shown in Fig. 8a–c. The wind and wave conditions for these events are summarised in Table 2. In each case, the measured wind direction is more nearly parallel to the coast than is the model wind direction. The differences between the three cases are caused mostly by the differences in wind direction. In example (a), the model winds are almost exactly offshore whereas the winds were measured to be 25° more southerly. The buoy shows some wave energy refracted round Spurn Head arriving at an angle of about 30° to the coastline. In example (b), the model winds are more southerly than they were in example (a) and some energy is arriving from the southerly along shore direction. The measured wind is this time 16° more southerly than the model wind so the model again underestimates the wave energy

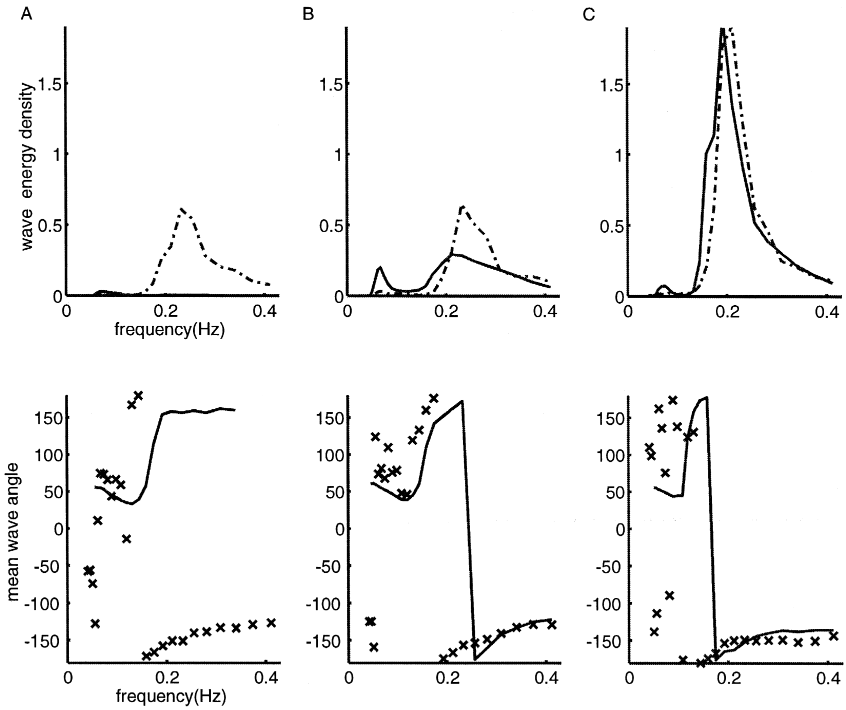

Fig. 8. Spectra at N3 for three events with offshore to southerly winds. The solid lines are the model data and buoy data is represented by dot-dashed lines in the top plots and by crosses in the bottom plots.

arriving at N3. In example (c), both model and buoy winds are from just east of south, so refraction is not required for energy to arrive at N3 and the waves are well modelled.

4.2.2.3. Fetch-limited growth. There were a few periods through the 2-month model run where offshore winds were fairly constant in speed and direction for a day or more, and the model and measured winds were in good agreement. In all these cases, the comparison between model and buoy wave spectra are also in quite good agreement indicating that the model is handling local growth well when given the correct forcing.

Table 2
Wind and wave conditions for events shown in Fig. 8a–c

	(a) 15:00 25th December 1994		(b) 00:00 16th January 1995		(c) 00:00 7th December 1994	
N3 Buoy H_S (m)/peak direction	1.10	−159.9	1.09	−161.3	1.66	−157.1
N3 Model H_S (m)	0.19		0.99		1.70	
Donna Nook wind speed/direction	10.8	−115	9.3	−125	12.9	−145
N3 Model wind speed/direction	9.8	−93	11.3	−109	14.7	−138

4.3. Summary

The results presented in Section 4.2 are typical of the model results for the 2-month period. Locally generated results are well modelled as long as the wind forcing is accurate but swell is often under-predicted. The wind forcing causes errors in the model in a number of ways. Inaccurate magnitude of the wind speed causes the expected under- or overestimates in local growth. Less obvious before this study was undertaken was how important errors in wind angle of the order of 10°–20° can be in coastal areas. The systematic error in wind direction from west of south caused wave energy to frequently be underestimated in the model.

The reasons for the underprediction of swell by the model have been shown by Hargreaves and Annan (1999) to be largely the fault of the model propagation scheme being unrealistically diffusive, but the smoothness of the wind forcing is also likely to be a contributing factor. A systematic error in the boundary forcing from the UKMO wave model is also seen to be of the order of 12% over the 2-month period of the run compared to the altimeter wave heights from TOPEX/POSEIDON.

The effects of the changing water depths and currents associated with the tide are observed at the N1 buoy station as a periodic variation of the significant wave height at frequent intervals throughout the 2 months. It is therefore important that the model should be re-run with a properly coupled hydrodynamic-wave model. Strong currents should have the effect of decreasing the bottom orbital velocity of the waves, so this means that the amount of suspended sediment may be overestimated in this case. The changing water depths will significantly affect the bottom friction in shallow water with consequences for the wave heights and sediment suspension. It is most likely this latter effect which is seen in the wavelet transform of significant wave height; the currents are expected to have more effect on wave period than wave height.

The presence of complex wave fields and the combination of errors already outlined earlier in this paper make it difficult to validate the model source terms, such as bottom friction. As mentioned in Section 4.1.2, the bottom friction is sensitive to the bottom friction parameter derived from the grain size and bed form. Whilst it may be possible to ‘tune’ the model parameters to provide good results for a particular region, this is a dangerous procedure on which to embark since it may result in over-compensation for other model errors.

5. Combined tide and wave impacts on vertical profiles of turbulence and SPM, single-point modelling

The combined influence on bed stress of both wave, currents and their interactions are examined. Thence, the effect of these combined influences on SPM concentrations is simulated in a single-point model of localised erosion and deposition. Comparison of these model simulations with observations provides erosion coefficients applicable at Holderness.

5.1. Observations

For a 22-day period in October 1994, an S4DW electromagnetic current meter, mounted 80 cm above the sea bed, at S1, provided the current and wave data. A 10-cm path length beam transmissometer, positioned 50 cm above the bed was used to monitor SPM concentration. The flow is highly rectilinear, running parallel to the coast (NNW–SSE). A springs–neaps cycle is evident, as are the stronger flood phase flows (up to 70 cm s^{-1} compared with 40 cm s^{-1} on the ebb). Water depth varies from 12–14 m during neaps with a wider 10–16 m range at springs.

For much of the time H_S is less than 0.5 m and the wave period remained relatively constant around 6 s. However, there is a period of enhanced wave activity between days 289 and 297 where wave heights regularly reached 1.5 m and occasionally 2 m. Several days later (between days 306 and 310) and coinciding with spring currents, significant wave heights increased again to over 1.5 m.

SPM concentrations were high for much of the deployment, and the maximum recordable value (150 mg l^{-1}) was frequently obtained. The effects of wave activity are obvious with large increases in concentration during the two events described above. During calmer periods, quarter-diurnal tidal resuspension and semi-diurnal advection can be recognised and the resultant 'twin-peaks' signature is a familiar and identifiable trend.

Fig. 9 shows the time series of observed SPM distributions at the six PMP positions shown in Fig. 1 over a 15-day, spring–neap tidal cycle in January–February 1995. This figure indicates the anticipated sharp decrease in concentrations with increasing depths offshore but also significant long-shore variations between N1–S1, N2–S2 and N3–S3. Model results described in Section 3 indicate little cross-shore variability in tidal currents with a root mean squared value close to 0.3 m s^{-1}. Thus this offshore decrease results from some combination of: increasing water depth, decrease in wave orbital velocities at the sea bed or decreased availability of coastal sediments.

5.2. Model formulation

The single-point model uses prescribed surface slopes to generate the tidal currents which are then coupled with the observed wave field measurements to calculate wave-modified bed stresses which are then used in the calculation of resuspension rates. The model is forced from the sea surface elevation predictions of the UK shelf-wide 2D operational storm surge forecasting model (Section 3.1). Turbulence closure modelling involves dynamically active models that allow levels of vertical exchange of momentum and scalars to adjust to changing dynamical and stability conditions. Here, a 1D, two equation k-turbulence model is applied.

5.2.1. The k-ε turbulence closure model

A more complete description of the model used here is given by Baumert et al. (1997). The boundary conditions for momentum assume a slip condition at the sea bed, incorporating a roughness parameter dependent on grain size and bed form. Wind stress is assumed to be zero.

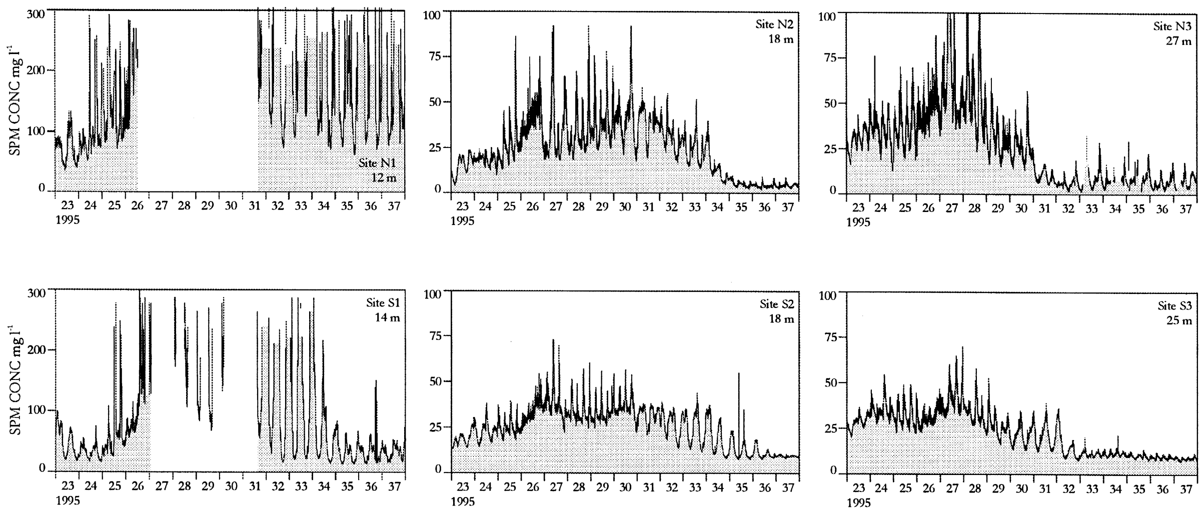

Fig. 9. SPM concentrations during 23/01/1995–06/02/1995 at sites N1, N2, N3 and S1, S2, S3.

The SPM submodel is designed to simulate the processes of sedimentation and erosion/resuspension. The material is assumed to be non-cohesive and only a single size class is implemented. The rates of erosion and deposition are dependent on the instantaneous bed friction velocity u_b^* so that for the SPM bottom boundary condition we have

$$\left[\phi w - \frac{\upsilon_t}{\sigma_\phi}\frac{\partial \phi}{\partial z}\right]_{\text{bed}} = j_s + j_e \tag{6}$$

where j_s and j_e represent the fluxes of SPM due to sedimentation and erosion, respectively. These two parameters are calculated using the formulas of Krone (1962) and Parthenaides (1965):

$$\text{sedimentation} \quad j_s = \phi_{\text{bed}} w \left[1 - \left(\frac{u_b^*}{u_e^*}\right)^2\right] \quad \text{for } u_b^* < u_e^* \tag{7}$$

$$\text{erosion} \quad j_e = M_{\text{ero}}\left[\frac{u_b^*}{u_e^*} - 1\right] \quad \text{for } u_b^* > u_e^* \tag{8}$$

u_b^* and u_e^* represent the critical friction velocities for the onset of sedimentation and erosion, respectively. No erosion or sedimentation occurs if the bed friction does not meet the specified limits. These critical friction velocities are prescribed at the beginning of the simulation in addition to the settling velocity and the M_{ero} erosion coefficient which is dependent on sediment type and bed history.

The effects of wave activity are incorporated via a modified bed friction velocity. The wave friction velocity u_w^* is calculated via the bed stress due to wave action τ_w:

$$\tau_w = \frac{1}{2} f_w \rho U_0^2 \tag{9}$$

where U_0 is the near bed orbital velocity and f_w is a wave friction factor, calculated using a semi-empirical expression (Jonsson, 1967; Jonsson and Carlsen, 1976):

$$\frac{1}{4\sqrt{f_w}} + \log_{10}\left[\frac{1}{4\sqrt{f_w}}\right] = -0.08 + \log_{10}\left[\frac{A_b}{k_b}\right] \tag{10}$$

k_b is the linear size of the roughness elements (= 30 z_0 is the roughness length) and A_b is given by U_0/ω, where ω is the angular frequency of the waves. A modified friction velocity due to the action of currents and waves (u_{cw}^*) is then calculated and used to derive an effective roughness k_{bc} 'felt' by the current at the bed (Grant and Madsen, 1979).

$$k_{bc} = k_b\left[24\frac{u_{cw}^* A_b}{u_w^* kb}\right]^p \tag{11}$$

where $p = 1 - u_c^*/u_{cw}^*$.

Wolf and Prandle (1999) used data at N2 for the entire 1994–1995 period to examine the effective wave-current bed stress coefficient, k. The ratio of tidal current amplitude to tidal elevation amplitude was found to decrease by up to 50% with increasing wave currents at the sea bed. The theory of Prandle (1982) was then used to determine the respective increase in bed friction coefficient required to produce these observed reduced tidal currents. A maximum increase in the effective value of k of 3.2 was calculated.

To solve the differential equations, the model uses a three-point, two-layer finite difference scheme on a staggered, non-equidistant grid permitting greater resolution in the near-bed region (Baumert and Radach, 1992; Burchard and Baumert, 1995).

5.3. Model results

5.3.1. SPM

Fig. 10 shows a comparison of observed and simulated near bed SPM concentration for the first deployment (days 284–312) at the inshore site N1. The upper panel (Fig. 10a) shows the results of a 24-h running mean applied to each of the datasets. This

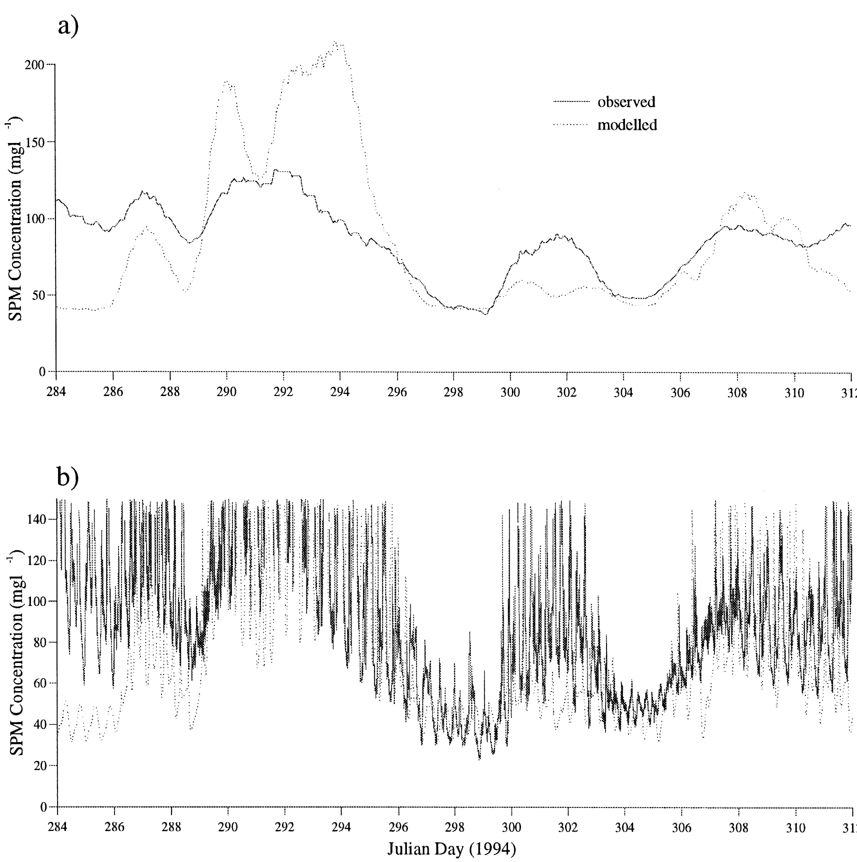

Fig. 10. Observed and modelled SPM concentrations: (a) 25-h filter, (b) no filter.

permits an examination of the model's capability to predict long-term changes in SPM levels, i.e., excluding the effects of diurnal tidal variation and individual wave events. The lower panel (Fig. 10b) compares the 1-min transmissometer results with the model's results which are written every 10 min.

Fig. 10a shows a generally favourable comparison between the model results and transmissometer measurements. The 24-h running mean shows primarily the response of SPM concentration to relatively low frequency, time scales O(few days), changes in the wave field. Four discernible maxima can be seen in both the observations and the model output around the time of enhanced wave activity.

During the first few days of the experiment, the predicted SPM concentration is constant and significantly lower than observed levels, which appear to be reducing. This indicates that perhaps there was a significant wave activity at this site prior to the deployment of the instrumentation.

Conversely, the model is overestimating the concentrations between days 289 and 296, a period when waves were very high (> 1.5 m). However, it is probably the case

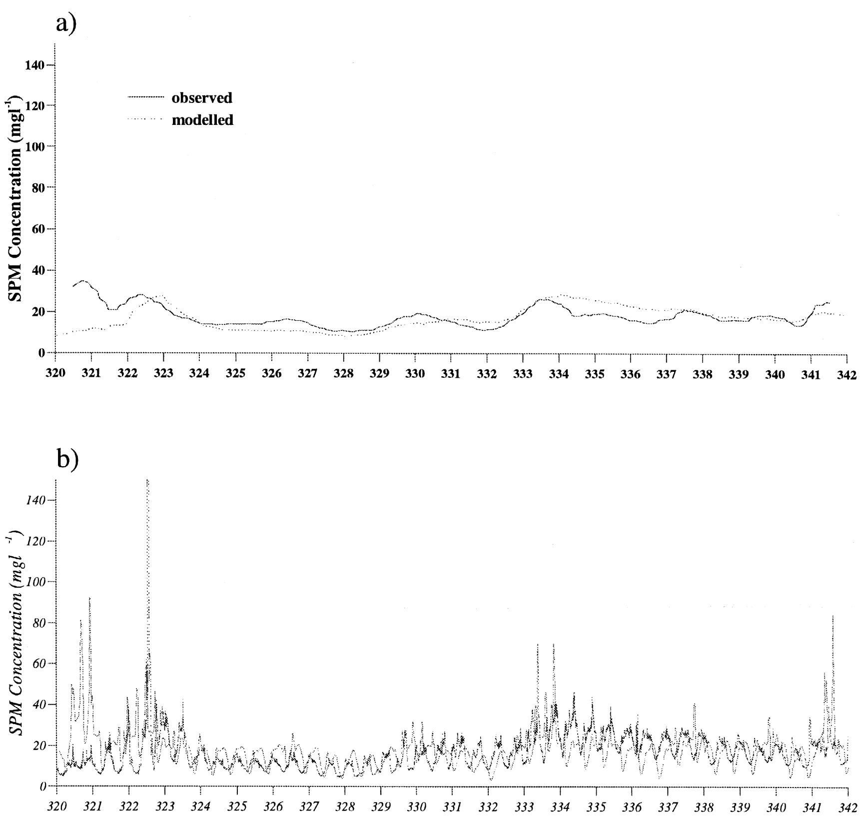

Fig. 11. Observed and modelled SPM concentrations: (a) 25-h filter, (b) no filter.

that, rather than over-predicting concentrations, the transmissometer is unable to record such high levels of suspended particulates.

Fig. 11 shows similar observed and computed SPM concentrations corresponding to a more quiescent period. Turning to the high frequency results (Figs. 10b and 11b), the extent to which wave activity dominates the SPM signal during the first deployment is clear and enhanced resuspension during stormy periods is reproduced although tidal variations are also evident throughout the observational period. For much of the longer second deployment, the calmer conditions mean that SPM variations are primarily due to a combination of advection and resuspension/settling driven by the semi-diurnal tidal flow.

5.3.2. Currents

Fig. 12 shows the wave statistics and modelled currents for a week at site N1. These results provide an excellent test of the model's ability in terms of the mean flow

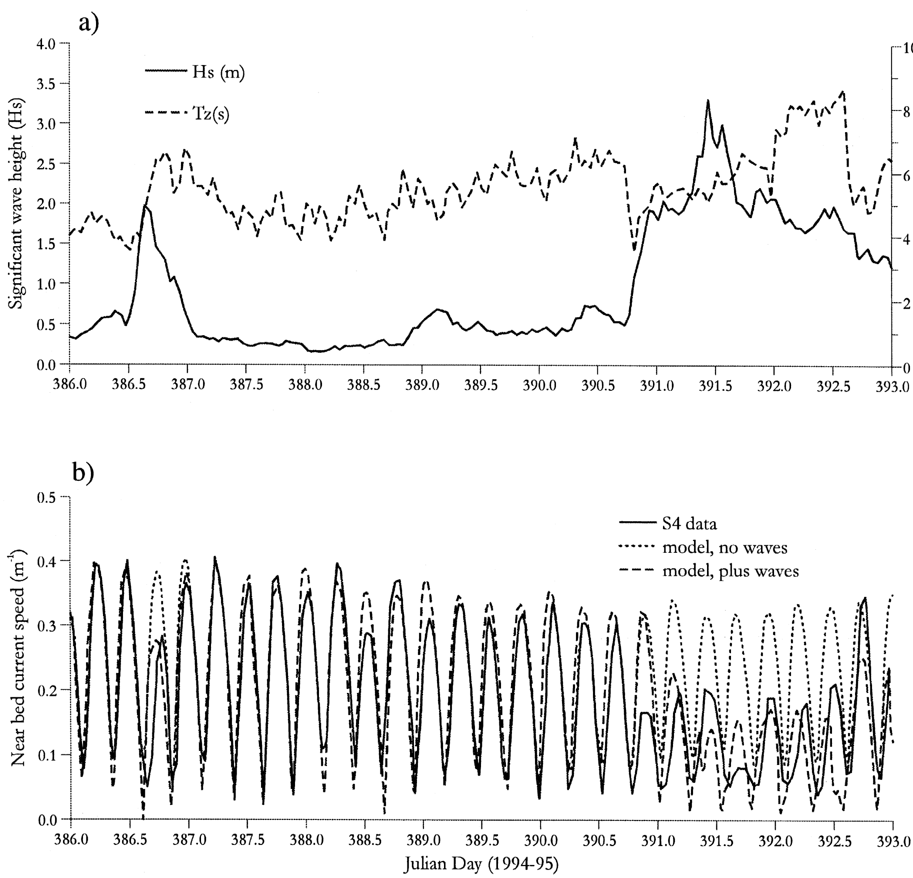

Fig. 12. (a) Observed H_S and T_Z at N1. (b) Near bed currents at N1; observed (S4); modelled, with and without waves.

simulation. There are two significant wave events during this period: a short burst (approx. 10 h) of enhanced wave activity (H_S up to 1.5 m) and a longer period of very high waves (up to 3 m) between days 391 and 393.

The current results presented include the S4 measurements and two model results, one that does not include the effects of wave activity and one that does. If the waves are less than 0.5 m in height, they are assumed unimportant in modifying the near bed dynamics. The S4 results show a significant reduction in current speed around the time of increased wave activity, for a single tidal cycle during the first event and for two days during the more intense second event. Only with the inclusion of wave effects does the model reproduce this behaviour and, although predictions during the second event are lacking in some respects, the results are encouraging.

5.4. Summary

An important feature of the results presented is that both the tidal regime (quarter-diurnal resuspension and semi-diurnal advection) and the wave field are important in determining the distribution of SPM. Waves become very much the dominant forcing mechanism at the inshore sites (N1 and S1) when the significant wave height exceeds 1 m (or 10% of the total depth). However, even during very stormy periods, when concentrations increase more than 10-fold, a tidal signal is still evident. It is the interaction and feedback between these two controlling functions that provide a major challenge to modellers.

Although the model results and observations occasionally diverge, the results are encouraging with both the higher frequency signals and the longer-term (24-h average) variations broadly in agreement. The effects of increased bed stresses due to large waves are clearly seen in the simulated SPM signal. Occasionally, the tidal signal disappears from the simulation, which is rarely the case in the observations.

A limiting factor in the model's performance is likely to be the sediment population, which is assumed to consist of a single size class of non-cohesive particles. A more complex parameterisation of the sediment population (i.e., additional size classes, aggregation) may lead to an improvement in performance, especially with more quiescent bed conditions. Energetic wave and current activity near the bed probably means that these factors are less important during these events.

6. SPM modelling off Holderness — impacts of tides and waves

6.1. Sediment transport model

A 2D (depth-averaged) sediment transport model, developed originally as subroutines for advection, dispersion, deposition and erosion of suspended particulate matter (SPM) in a 3D model of the southern North Sea (James et al., 1998), is applied here to the UK East Coast. The basis for this model is the pre-operational hydrodynamic model described in Section 3, both models being defined on the same 1.2-km Cartesian grid.

6.1.1. Sediment suspension and deposition

The rate of deposition and resuspension of sediment in this model is controlled by a number of parameters, the values of which relate to the amount (i.e., concentration) and type (i.e., particle size, settling velocity) of the material. Deposition of SPM occurs only if the value of the shear stress acting at the bed, τ_{bed}, falls below some predefined critical value, $\tau_{cr,dep}$. The rate of deposition, per unit area of bed, is modelled by:

$$(1-\tau_{bed}/\tau_{cr,dep})c_{bed}W_{50} \tag{12}$$

where C_{bed} is the SPM concentration very close to the bed (g m^{-3}) and W_{50} is the median settling velocity of the SPM (m s^{-1}).

Similarly, resuspension of deposited sediment occurs only for as long as the value of the bed shear stress exceeds some other critical value, $\tau_{cr,ero}$. The rate of resuspension, per unit area, is modelled via

$$M_{ero}(\tau_{bed}/\tau_{cr,ero}-1) \tag{13}$$

where M_{ero} (g m^{-2} s^{-1}) is a constant, which for a particular sediment type, defines the mass of sediment eroded from a unit area of bed each second.

An important feature of this model is that it simulates the effect that surface waves have upon the SPM deposition and resuspension processes — note that the effects upon the sediment transport as a whole are not simulated, as the hydrodynamic model is not coupled to the wave model. The model calculates the component of the bed shear stress due to waves. Linear wave theory is used to calculate the wave orbital velocity from modelled wave height (H_S) and period (T_Z). Associated wave-induced stress is then calculated incorporating the bed roughness length obtained from a digitised map of bed sediment type. This component of the bed shear stress is added to the component of shear stress due to currents, in order to give a total bed shear stress.

6.1.2. Model forcing

The model is forced at its boundaries by water levels and currents interpolated from POL's 12-km hydrodynamic model. Meteorological data, i.e., hydrostatic pressures and wind stress components, are interpolated from the UKMO's 50-km Limited Area Model. The sediment transport model is driven with hourly values of currents and elevations, stored at each model grid point from previous simulations with the hydrodynamic model, and interpolated to the time step of the sediment model. The simulations reported in this paper concentrate on the period between October 1994 and February 1995, this being the period for which the most complete SPM data set exists.

6.1.3. Model simulations

The Holderness coastal erosion is simulated by a continuous release of sediment into the water column from a land based coastal strip. This coastal strip also forms the basis of a bed source of sediment which, under certain conditions, is released into the water column via resuspension. The seabed of the whole of this region is also treated as a potential resuspension source.

6.2. Observations

In addition to the in situ measurement of SPM described earlier, remote sensing imagery of surface/SPM was used to verify the modelled distributions. Ten CASI (Compact Airborne Spectrographic Imager) images of the Holderness Coast and Humber estuary were obtained from the UK Environment Agency (EA). The images were collected during the summer months (May 1994–September 1995), as part of the EA's routine monitoring programme of UK coastal waters. The spatial resolution of CASI is dependent on the altitude of the aircraft on which it is carried, and is typically between 5 and 20 m, i.e., the pixel size of the resulting image varies between 25 and 400 m^2. For the Holderness coastline, a 5.5-km wide strip is thus covered in some detail.

For an indication of the suspended matter distribution on a more regional scale, 18 relatively cloud free images produced by the MOS (Modular Optoelectronic Scanner) scanner have been obtained. MOS has a swath width of 200 km, and a pixel size of 0.52 km^2. The resolution of these images is thus of the same order of magnitude as the Holderness numerical models (1.2 km, equivalent to a pixel size of 1.44 km^2). The range of MOS images obtained for PROMISE covers the period between March and June in the years 1996–1998, so unlike the CASI images there is some overlap with data from the Holderness Experiment and consequently contoured model output can be quantitatively compared with the images.

6.3. Results

An extensive set of numerical simulations was undertaken to determine the sensitivity of computed SPM concentrations to the precise location and rates of cliff supply and, likewise, the dependency of a specific simulation on prior chronology. Details of this experimentation are omitted but a general conclusion is that accurate distribution of surficial sediments within the Holderness region requires 'run-in' simulations of about 1 year.

Fig. 13 shows computed the SPM time-series over a 2-month period starting 1/12/94 at the PMP locations shown in Fig. 1. These simulations are for sand and silt with fall velocities $w_s = 10$ mm s^{-1} and $w_s = 0.1$ mm s^{-1}. The latter value is optimised to best fit the observations shown. The simulations show the time series for tide-surge alone and with wave-enhanced bed stress (using wave data from the simulations described in Section 4 and wave-current interaction formulations as described in Section 5).

The predominance, throughout, of semi-diurnal modulation is indicative of the advection of pronounced lateral gradients in SPM. Fig. 14 indicates the corresponding computed instantaneous spatial distributions, confirming the magnitude of these gradients.

The instantaneous spatial distribution for sand illustrates how the suspension and subsequent movement is severely restricted compared to that for silt. Fig. 15 shows examples of 'instantaneous' SPM distributions obtained from the CASI (Shimwell, 1998) indicating broad agreement with the patterns shown in Fig. 14. Since the CASI measures surface concentrations, the image will correspond to finer particles in all but the shallowest water depths.

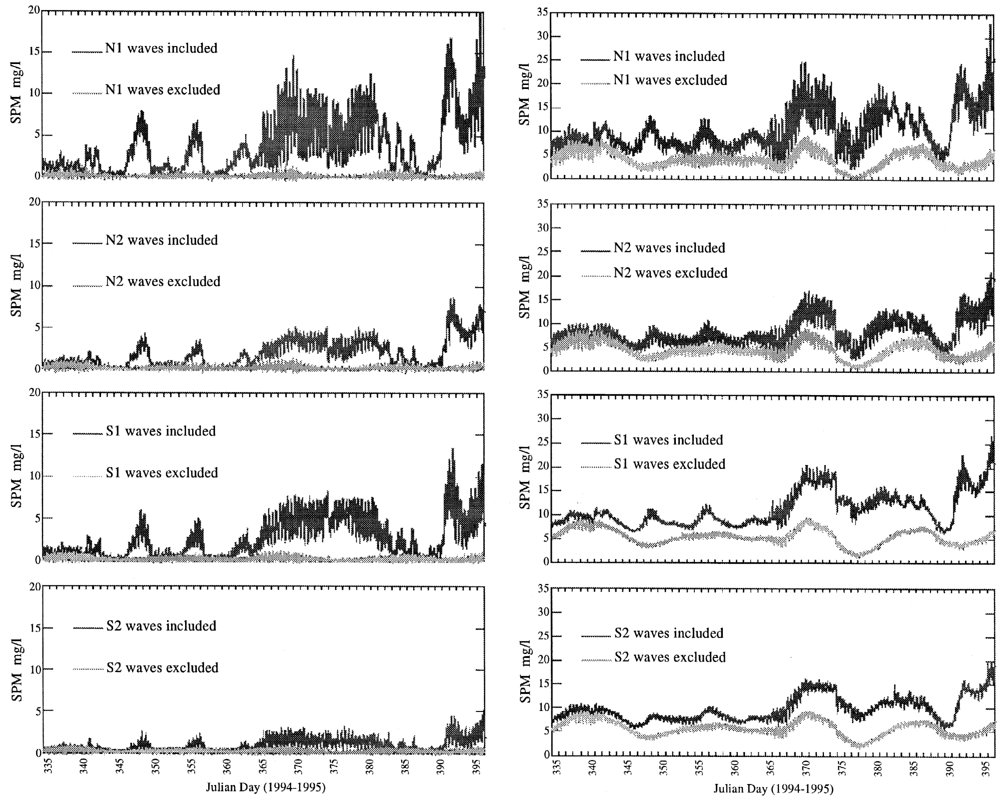

Fig. 13. Suspended sediment dynamics at sites N1, N2, S1 and S2 (Holderness area) December 1994–January 1995 for an eroding bed source of: sand with $w_s = 10$ s^{-1} (left); silt with $w_s = 0.1$ mm s^{-1} (right).

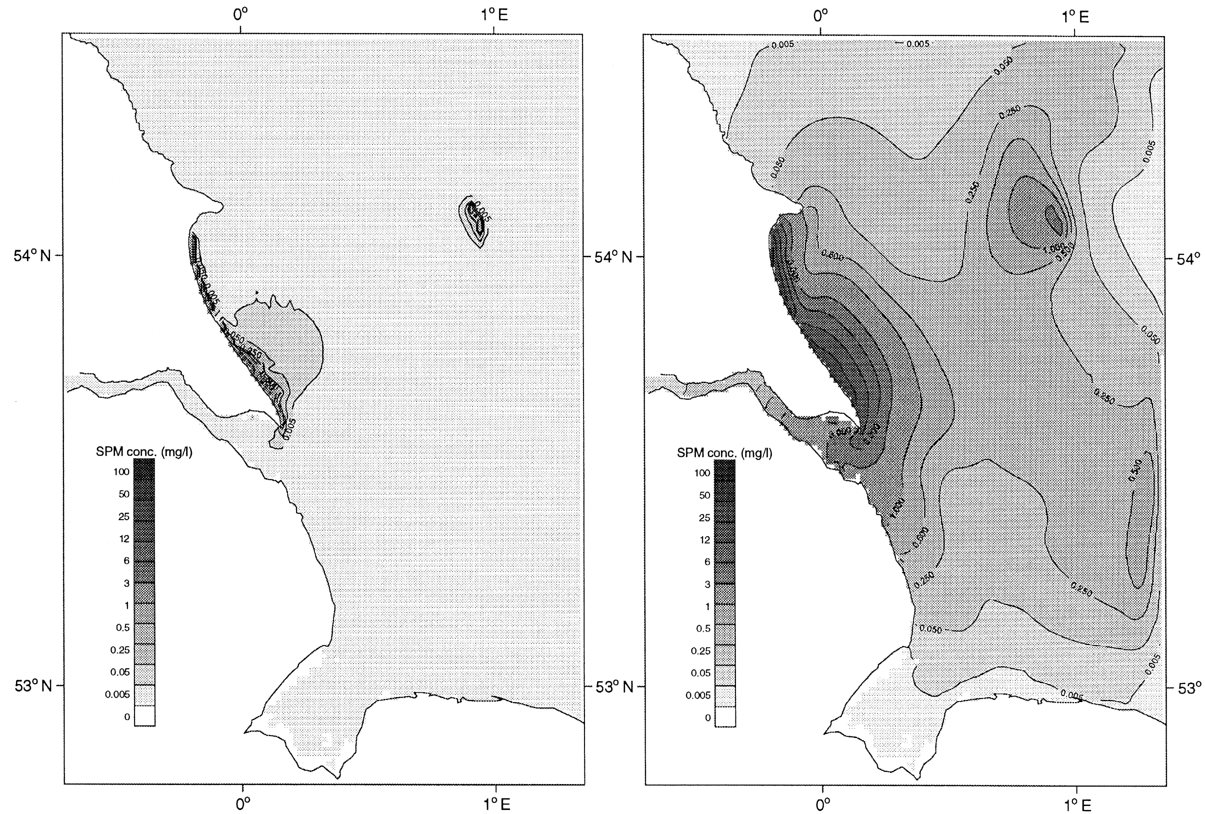

Fig. 14. Simulated suspended sediment distribution at 0:00 on 30/9/1994 following a 21-month spin-up, coastal strip source eroding at a rate of 10^9 kg year^{-1} for: sand with $w_s = 10$ mm s^{-1} (left); silt with $w_s = 0.1$ mm s^{-1} (right).

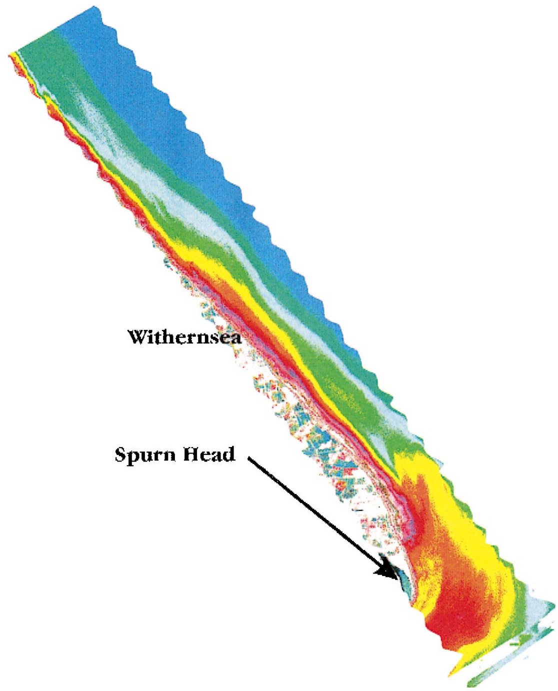

Fig. 15. CASI image of the Holderness coast, 21st September 1995 09:50 LW + 30 min. (Raw image courtesy of the Environment Agency.)

6.4. Summary

The SPM simulations of coastal erosion at Holderness are essentially exploratory. In general, accurate reproduction of observed SPM time-series (as in Fig. 9) is not possible given the interdependencies of: uncertain rates and locations of coastal supply of differing sediment types, resulting chronologies of surficial sediments, consequent dependencies of wave-current bed stress and, ultimately, variability of vertical SPM profiles reflecting all of the latter and associated turbulence profiles.

However, the characteristic features of the observations are reproduced including realistic representations of the respective influences of tides and waves. Thus, quantitative estimates of the varying impacts of the latter can be made including useful sensitivity analyses of how such balances may change under varying climate change scenarios of varying mean sea level, wave climate and surge occurrences.

7. Conclusions

The observational data set from the Holderness Experiment has been widely used for both process studies and as a bench-test for model formulation and validation in simulating tidal currents, waves and SPM distributions. The experiment provided useful general experience of the suitability of a range of in situ radar, aircraft, and sea-borne sensors and instrumentation systems. For currents and waves, close agreement is found between the observations and model simulations, whereas for SPM observations only a limited agreement with modelling is found.

Locally generated waves are well modelled as long as the wind forcing is accurate but swell is often under predicted. This study shows how important errors in wind angle of the order of 20° can be in coastal areas. From the point of view of sediment transport, it is the large low frequency wave events that have the most impact. Since the sum of wave and current bottom stress is used to calculate sediment suspension, both size and timing are important. The diffusive nature of the model propagation scheme causes an 'external' event of, say, 4 h duration to spread into, typically, an 8-h event of much smaller magnitude by the time it reaches the coast (Hargreaves and Annan, 1999).

In Section 5, it was shown that in the shallowest water (< 15 m), waves become the dominant mechanism in sediment suspension whenever $H_S > 1$ m. However, modulation of the tide by waves and vice versa is significant in such shallow water and interactive wave-tide modelling is required. Impacts of such interaction on near-bed tidal currents have been examined using point-modelling simulations. Comparisons of these simulations with observations indicate that existing models incorporating conventional bed stress formulations and turbulence representations can reproduce these processes accurately. However, detailed simulations of SPM time series is more difficult. One particular difficulty highlighted was the need for a complex representation of sediment population (the associated problems of flocculation and disaggregation are not considered here). In Section 6, preliminary modelling aimed at applying the results from these tidal, wave, turbulence and SPM modelling components to simulate sediment fluxes offshore of Holderness. Results indicate rapid export of fine material ($w_s = 0.01$ mm s^{-1}) compared with limited movement of coarser material ($w_s = 10$ mm s^{-1}). Movement of the latter being confined to those few days a year of maximum wave activity.

The broad objectives of reproducing the sediment fluxes off Holderness and relating these to tidal and wave forcing have been achieved. However, accurate computation of these fluxes remains sensitive to largely empirical coefficients used in determining erosion and deposition rates. Bed roughness strongly influences both these coefficients and the associated near-bed current magnitudes (including wave impact thereon). This parameter can change significantly over a tidal cycle and dramatically over seasons or in the course of a major event. Accurate simulation of sediment fluxes on a day-to-day basis is constrained by dependency on the initial distribution of mobile sediments. The latter depends on rates and locations of original sources and the time history of preceding events. Remote sensing via aircraft could provide data for assimilation into such models to circumvent these constraints.

The approaches developed here can be readily applied to other coastal regions to indicate the likely distributions and pathways of known sediment sources. However quantitative simulations will require an associated observational programme. A subsequent stage is to understand the evolving balance between the forecasted sediment movement — the resulting morphological adjustments and thence modifications to the prevailing tidal current and wave regimes.

Acknowledgements

The Holderness Experiment originated as part of the (UK) NERC's LOIS project. The comprehensive data set subsequently contributed and was supported by a number of related studies, namely: (i) CAMELOT (contract FD311 of MAFF's Flood Defence Commission with NERC); (ii) SCAWVEX — Surface Current and Wave Variability Experiment. MAST II (coordinator: L. Wyatt, University of Sheffield.) (MAS2-CT940103); (iii) PROMISE — PRe-Operational Modelling in the Seas of Europe. MAST III (coordinator: D. Prandle, Proudman Oceanographic Laboratory.) (MAS3-CT950025).

Hydromod would like to thank also the Bundesamt für Seeschiffahrt und Hydrographie (BSH) and the Deutsche Wetterdienst (DWD) for the valuable assistance in providing meteorological and hydrographic forecast data for the North Sea.

References

Allender, J., Audunson, T., Barstow, S.F., Bjerken, S., Krogstad, H.E., Steinbakke, P., Vartdal, L., Borgman, L.E., Graham, C., 1989. The WADIC project: a comprehensive field evaluation of directional wave instrumentation. Ocean Eng. 16, 505–536.

Baumert, H., Radach, G., 1992. Hysteresis of turbulent kinetic energy in nonrotational tidal flows: a model study. J. Geophys. Res. 97, 3669–3677.

Baumert, H., Reneger, M., Szilagyi, B., 1997. The generic model: 1D turbulence-SPM-wave model. Proudman Oceanographic Laboratory Report No. 47.

Burchard, H., Baumert, H., 1995. On the performance of a mixed layer model based on the k-ε turbulence closure. J. Geophys. Res. 100 (C5), 8523–8540.

Duwe, K., Hewer, R., Backhaus, J.O., 1983. Results of a semi-implicit two-step method for the simulation of markedly nonlinear flows in coastal seas. Cont. Shelf Res. 2 (4), 255–274.

Grant, W.D., Madsen, O.S., 1979. Combined wave and current interaction with a rough bottom. J. Geophys. Res. 84 (C4), 1797–1808.

Graber, H.C., Madsen, O.S., 1988. A finite-depth wind-wave model: Part 1. Model description. J. Phys. Oceanogr. 18, 1465–1483.

Hargreaves, J.C., Annan, J.D., 1999. The impact of fierce weather on lazy modelling. Proceedings of the Air–Sea Interface Symposium, 11–15 January 1999, Sydney, Australia. In press.

Hasselmann, K., 1968. Spectral dissipation of finite depth gravity waves due to turbulent bottom friction. J. Mar. Res. 26 (1), 1–12.

James, I.D., Proctor, R., Holt, J.T., McManus, J.P., 1998. Transport and dispersion modelling of shelf seas. Final report for NORMS 42 GST/02/745. LOIS Special Topic Final Report. Proudman Oceanographic Laboratory. LOIS publication No. 530.

Jonsson, I.G., 1967. Wave boundary layers and friction factors. Proc. 10th Coastal Eng. Conf. 1, 127–148.

Jonsson, I.G., Carlsen, N.A., 1976. Experimental and theoretical investigations in an oscillatory turbulent boundary layer. J. Hydraul. Res. 14 (1), 45–60.

Komen, G.J., Cavaleri, L., Donelan, M., Hasselmann, K., Hasselmann, S., Janssen, P.A.E.M., 1994. Dynamics and Modelling of Ocean Waves. Cambridge Univ. Press.

Krogstad, H.E., Barstow, S.F., 1999. Satellite wave measurements for coastal engineering applications. Coastal Eng. 37 (3–4), 283–307.

Krone, R.B., 1962. Flume studies of the transport of sediment on estuarial shoaling processes. Report, Hydraulic Engineering Laboratory, University of California, Berkeley.

Lane, A., 1997. Currents and SPM (suspended particulate material) measurements. Holderness, East Coast, England November–December 1993, October 1994–February 1995 and October 1995–January 1996. Proudman Oceanographic Laboratory Report No. 45, 50 pp.

Lane, A., Riethmüller, R., Herbers, D., Rybaczok, P., Günther, H., Baumert, H., 2000. Observational data sets for model development. This volume.

Monbaliu, J., Padilla-Hérnandez, R., Hargreaves, J.C., Carretero Albiach, J.C., Luo, W., Sclavo, M., Günther, H., 2000. The spectral wave model WAM adapted for applications with high spatial resolution. This volume.

Parthenaides, A., 1965. Erosion and deposition of cohesive soils. J. Hydraul. Div., ASCE 91, (HY1).

Player, R.J., 1996. H.F. Radar (OSCR) surface current measurements, Holderness, East Coast, England. September 1994–March 1995. Proudman Oceanographic Laboratory Internal Document No. 92. Unpublished manuscript.

Prandle, D., 1982. The vertical structure of tidal currents and other oscillatory flows. Cont. Shelf Res. 1, 191–207.

Prandle, D., Ballard, G., Banaszek, A., Bell, P., Flatt, D., Hardcastle, P., Harrison, A.J., Humphery, J., Holdaway, G., Lane, A., Player, R., Williams, J.J., Wolf, J.,1 996. The Holderness coastal experiment ’93–’96. Proudman Oceanographic Laboratory, Report No. 44, 48 pp.

Shimwell, S., 1998. Remote sensing of suspended sediment off the Holderness Coast, UK. ARGOSS Report A5 23 pp. (unpublished).

van Rijn, L.C., 1993. Principles of Sediment Transport in Rivers, Estuaries and Coastal Seas. Aqua Publications, Amsterdam.

Wolf, J., 1998. Waves at Holderness: results from in-situ measurements. Proceedings of Oceanology ’98, Brighton, UK. pp. 387–398.

Wolf, J., Prandle, D., 1999. Some observations of wave-current interaction. Coastal Eng. 37 (3–4), 471–485.

Wyatt, L.R., Thompson, S., 1998. Evaluation of H.F. Radar wave measurements. Proceedings of Oceanology ’98, Brighton, UK. pp. 435–444.